





Article

Role of particle gradation of clay–sand mixtures on the interfacial adhesion performance of polymer coatings

Nidhi Murali¹, Jing Li² , Anvi Agarwal¹, Patrick Berthault²  and Pijush Ghosh¹

¹Department of Applied Mechanics and Biomedical Engineering, Indian Institute of Technology Madras, Chennai, India and ²Université Paris-Saclay, CEA, CNRS, NIMBE, 91191, Gif-sur-Yvette, France

Abstract

The interface performance between clay–sand mixtures and concrete structures is governed by the mixture's composition and its physical properties. Moisture content and particle-size distribution play important roles in deciding the mixture's arrangement of soil particles, porosity, hydraulic conductivity and behaviour under various mechanical loadings. Application of a polymer interfacial coating can improve the bond performance between soils and concrete mainly *via* interfacial friction/mechanical interlocking. The present work analyses the development of interfacial strength between clay–sand mixtures and a polymer coating with changes in particle gradation. The multi-scale mechanisms at the interface are investigated, giving primary attention to soil porosity. A 50:50 clay–sand mixture exhibited a greater interfacial adhesive performance compared to other soil mixtures. In addition, the moisture-controlled pores and gradation-controlled pores demonstrated differences in macroscale interfacial strength. Both mercury intrusion porosimetry (MIP) and ¹²⁹Xe nuclear magnetic resonance (NMR) were utilized to detect the pore structure of the mixtures. ¹²⁹Xe-NMR revealed the pore distribution of the mixtures as ranging from macropores to nanopores, and MIP complemented the pore information by determining the critical pore entry diameter in the macropore regime. Mesopores dominated with increasing fine sand content until a threshold value was reached; thereafter, merging of pores occurred and macropores dominated.

Keywords: ¹²⁹Xenon NMR; interfacial adhesion; microstructure; MIP; porosity

(Received 10 January 2024; revised 28 February 2024; accepted 29 February 2024; Accepted Manuscript online: 14 March 2024)

The formation of the soil–structure interface guides the overall performance of such a structural system. For geotechnical works, cast-*in-situ* interface formation is greatly preferred. In this, the cement grout is either directly cast or pressure grouted between compacted soil and structural material such as in pre-bored driven piles (Wang *et al.*, 2020; Wu *et al.*, 2023). Furthermore, interface formation is affected by numerous parameters ranging from macroscale features such as asperities and undulations on surfaces to microscopic features such as porosity, chemical interactions and surface energy, amongst others. The mechanical strength of an interface is affected by the surface roughness, surface texture and the materials that are in contact (Di Donna *et al.*, 2016; Pan *et al.*, 2023). The shear behaviour of an unsaturated soil–concrete interface is affected by matrix suction values. A lower water content favours higher matrix suction and thereby higher interface shear performance (Chen & Liang, 2024). Conditioning of clay bricks for a period of 30 min increased the shear bond strength with mortar (Briceño *et al.*, 2024). The importance of moisture content in driving interface shear characteristics is highlighted in most of the abovementioned works.

Studies on interfacial behaviour between polymer coatings and clay/cement substrates revealed adhesion mechanism at different

length scales (Gujar *et al.*, 2021, 2023; Ilango *et al.*, 2021; Murali *et al.*, 2022). Biopolymers and cationic polyacrylamide are widely used for soil stabilization applications, and they have proved to be effective in freeze–thaw settings (Orts *et al.*, 2007; Soltani-Jigheh *et al.*, 2019). A hydrating cement surface exhibited a comparable adhesive strength (2–3 MPa) for an epoxy coating at 2 and 28 days of hydration, whereas sodium bentonite (Na-Bt) clay exhibited interface adhesive strengths in the range of 400–500 kPa. Epoxy aided in interface formation in each of the cases through various mechanisms. In the case of clay, diffusion of the polymer into the clay macropores at the surface coupled with hydrogen bond interaction between epoxy and oxygen donor sites on the clay surface predominated. For cement, physical interaction between cement hydrates (C–S–H, CH) and epoxy groups drives the interface formation. As understood from previous studies, pores in clay plays major role in interface formation. The nature of the deposition and particle gradation gives rise to inherent porosity in a clay. However, the porosity in a clay can be affected by other environmental factors and also the proximity of the structural component. For example, changes in porosity at the interface of cement and clay even at a distance of ~2 mm due to dissolution and precipitation reactions within a barrier system were reported by Shafizadeh *et al.* (2020). Moreover, moisture content alters the soil porosity, and this effect is predominantly seen for clayey soils (Feng *et al.*, 2018). Hence, it is important to study porosity variation in clay–sand mixtures and its contribution to interface formation with a polymer coating in the context of a soil–structure interface.

Corresponding author: Pijush Ghosh; Email: pijush@iitm.ac.in

Cite this article: Murali N, Li J, Agarwal A, Berthault P, Ghosh P (2024). Role of particle gradation of clay–sand mixtures on the interfacial adhesion performance of polymer coatings. *Clay Minerals* 59, 63–72. <https://doi.org/10.1180/clm.2024.7>

A remarkable improvement in the geotechnical properties of clay was achieved with the incorporation of lime-zeolite. The stabilization mechanism altered the microstructure of the clay and contributed towards improved mechanical properties, as explained in Khajeh *et al.* (2023). Any additive, be it conventional stabilizers or polymers, improves the properties of the clay significantly at the macroscale by changing the pore microstructure in the clay (Xia *et al.*, 2023). Considering this aspect, the current study looks at the porosity effect on the interfacial strength performance of polymer-coated clay–sand mixtures.

The particular focus of this study is on clay–sand mixtures. The behaviour of clay–sand mixtures under compressive loading is governed by their sand content. The effective load-bearing capacity of these mixtures is guided by the threshold fine sand content, which forms a sand skeleton within the matrix. However, addition of a greater clay content could interfere with the hydraulic conductivity of the mixture (Watabe *et al.*, 2011; Tripathi & Viswanadham, 2012). Clay–sand mixtures, especially those present as sediments in estuaries and tidal inlets, amongst others, exhibit inter-fractional (sand–clay) interactions that affect their transport properties such as deposition, erosion and so on (Cuthbertson *et al.*, 2018). Our previous work explaining the microstructural mechanism of epoxy-coated Na-Bt revealed the formation of a diffuse interface between the epoxy and clay, primarily resulting from epoxy percolation into clay surface pores (Murali *et al.*, 2022). However, under field conditions, profound variation in the particle sizes of soil exists, and this could significantly affect their porosity. To clearly understand the effects of variation in soil porosity on interfacial adhesive strength, different clay–sand compositions are considered in this study.

A wide range of techniques such as cryo-scanning electron microscopy (cryo-SEM; Lubelli *et al.*, 2013) and mercury intrusion porosimetry (MIP; Duan *et al.*, 2013) are used to estimate the pore-size distribution and pore connectivity of soil systems. However, conventional techniques pose numerous challenges, as most of them are destructive techniques. Usage of imaging techniques such as SEM to analyse the porosity changes in reinforced soils under drying–wetting cycles was reported by Hou *et al.* (2021), and the use of field emission SEM to study the porosity of gas/liquid plays in China was reported by Zhu *et al.* (2023). Various advanced nuclear magnetic resonance (NMR) techniques were also used to understand the pore structure of soil, such as

^1H -NMR relaxometry (Carrero-González *et al.*, 2012), magnetic resonance imaging (MRI) and ^{129}Xe -NMR (Tsiao *et al.*, 1998; Filimonova *et al.*, 2011).

Both ^1H -NMR relaxometry and MRI require a high water/solvent content and normally require full saturation inside samples to obtain a high signal-to-noise ratio, so they are not suitable for studying soil samples containing only small amounts of water. ^{129}Xe gas is a sensitive gas probe for NMR, which has been used to detect pore structure regardless of the water content of various construction materials, such as cementitious materials, shales and geopolymers (Li *et al.*, 2022). Hence, in this work, three clay–sand mixtures were prepared at moisture contents equivalent to their ‘dry of optimum’ as schematically shown in Fig. 1. ^{129}Xe -NMR and conventional MIP methods were applied to provide complementary information of the porous structures of the three mixtures. The interfacial performance of each mixture with a polymer coating with a thickness (t) of 4 mm (Fig. 1) was evaluated by analysing the shear load–displacement plot. The mechanisms were studied by taking into account the energy-release rate expression proposed by Hölck *et al.* (2012). The evaluation of the effects of various porosities (obtained by varying the gradation of the soil) on the interfacial bond strength of epoxy coatings is the specific objective of this work.

Materials and methods

Materials

Soil

The soils considered were Na-Bt and mixtures of Na-Bt and fine sand in the proportions 70:30 and 50:50 by weight. The optimum moisture content (OMC) and maximum dry density (MDD) of all of the mixtures were calculated by performing standard Proctor tests as IS 2720 Part VII-1974, and these are reported in Fig. 2a. Pure bentonite exhibited the highest OMC of 34.96%. As the sand content in mixture increased, the surface area of bentonite particles reduced for water absorption. Thus all clay–sand mixtures had lower OMCs than pure Na-Bt (Agus *et al.*, 2010). The particle-size distributions of the mixtures were evaluated by sieve analysis, and that of Na-Bt was evaluated by hydrometer analysis as per ASTM D7928-17. Particles of size $2\ \mu\text{m}$ were predominant in pure Na-Bt, with a percentage finer value of 80. These results are presented in Fig. 2b.

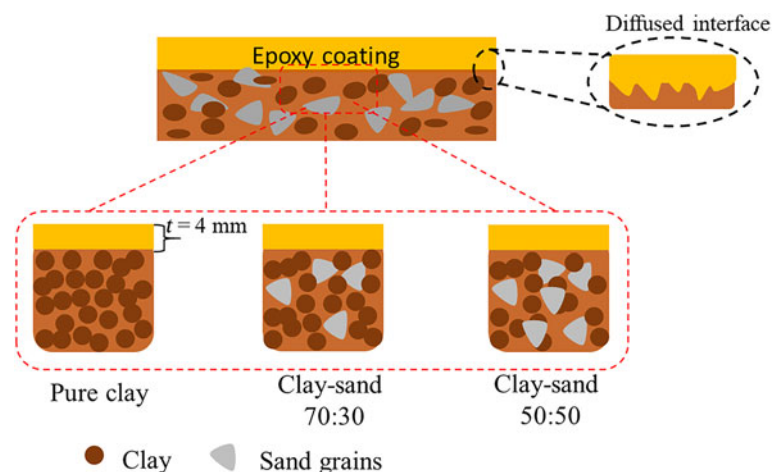


Figure 1. Schematic illustration of the epoxy-coated clay–sand mixtures considered in this study. The various pore spaces found in a clay–sand mixture are evaluated using MIP and ^{129}Xe -NMR.

Polymer

Bisphenol-A diglycidyl ether (DEGBA) resin and diethylene triamine (DETA) hardener were chosen as the polymer materials for usage as coatings over the compacted soil mass. The resin and hardener were used in the proportion 2:1 by weight over a curing period of 7 days at room temperature.

Preparation of compacted clay-sand mixtures

Each of the soil mixtures was statically compacted in a square cutter of size 60 × 60 × 25 mm at bulk densities of 1.755 and 1.773 g cm⁻³ corresponding to the ‘dry of optimum’ water content (i.e. OMC = 5%). One more sample of 60:40 clay-sand proportions (60C:40S) having a bulk density of 1.718 g cm⁻³ was also considered for the NMR studies. Representative samples for porosity studies were collected from the compacted specimens and lyophilized to preserve the porosity. Lyophilized samples were stored in vacuum desiccators until they were tested.

For measuring the interfacial adhesion between the compacted soil and epoxy coating, the samples were cast in a shear box of size

60 × 60 × 10.5 mm (Fig. 3). Two identical pieces were joined together, maintaining a gap of 4 mm, and epoxy resin was injected into this gap. The prepared sandwich composite samples were wrapped in cling film and kept in a vacuum desiccator for 7 days to allow for curing of the resin.

Mercury intrusion porosimetry

Macropores and mesopores in the compacted soil masses were estimated *via* MIP. The instrument used was a Pore Master 60 (Quantachrome, FL, USA) in the pressure range of 0.01–60 000 psi. The pressure interval was 0.028 psi, and data were recorded at a temperature of 23°C in order to reduce the evaporation rate of mercury. MIP works on the principle that the pressure at which mercury intrudes into a pore is inversely proportional to the pore’s radius. This is mathematically represented by Washburn’s equation (Equation 1) as

$$P = \frac{-4\gamma \cos \theta}{d} \tag{1}$$

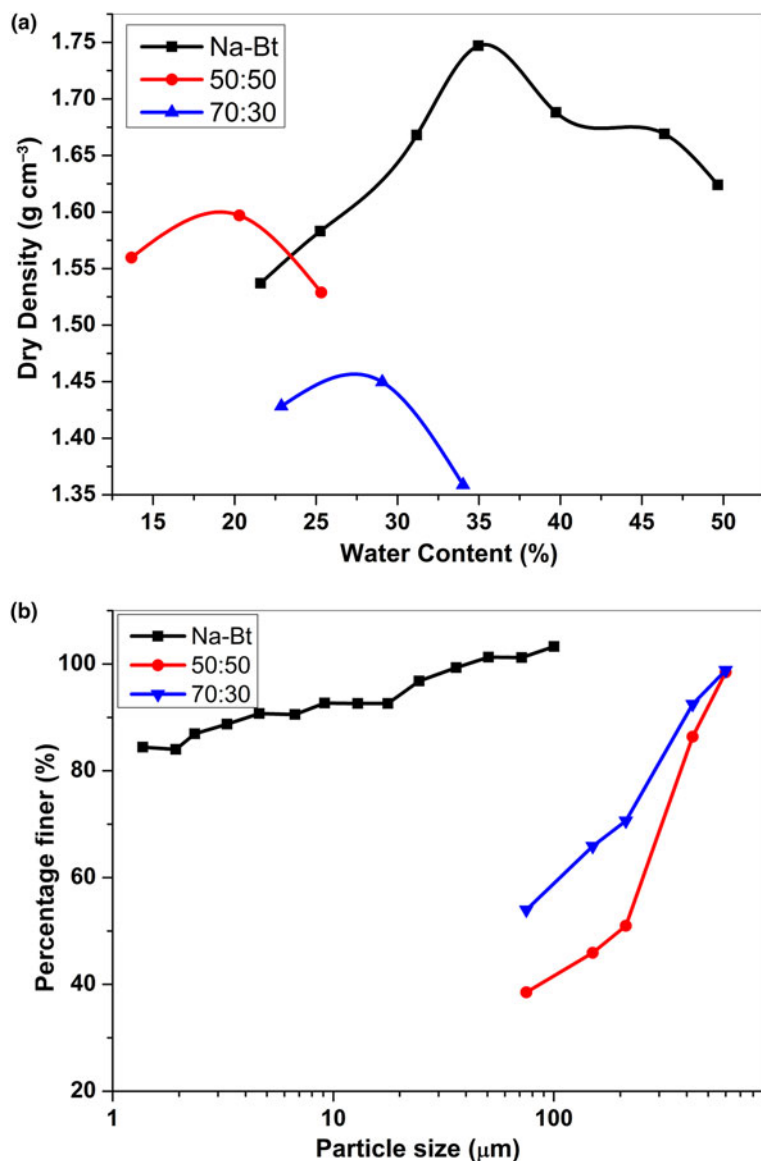


Figure 2. (a) Proctor curves of all of the mixtures obtained as per IS 2720 Part VII-1974. (b) Particle-size distribution of the clay-sand mixtures.

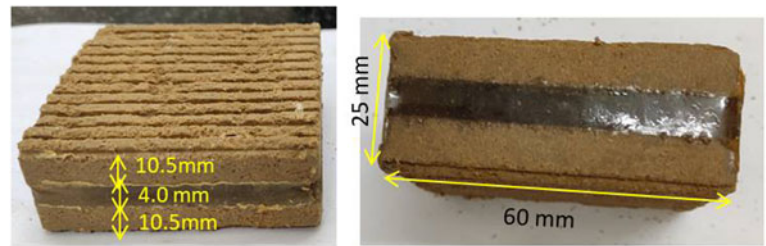


Figure 3. Clay-sand compositions coated with epoxy polymer prepared for shear testing. Curing of the resin for 7 days was followed by testing in a conventional direct shear apparatus.

where P is the pressure at which mercury intrudes in Pa, γ is the surface tension of mercury, θ is the contact angle of mercury taken as 140° and d is the entry diameter of the intruded pore in μm .

Samples prepared according to the methodology described in the ‘Preparation of compacted clay-sand mixtures’ section were considered for MIP studies.

^{129}Xe NMR study of the clay-sand composites

The Xe atom has a large electron cloud, which makes Xe gas an ideal probe gas for NMR experiments because its NMR parameters are sensitive to the chemical composition and the physical structure of its environment. ^{129}Xe chemical shifts reflect pore size and structure, as the chemical shift (δ) of ^{129}Xe in the porous medium without strong adsorption sites can be modelled as the sum of three major contributions (Equation 2):

$$\delta = \delta_0 + \delta_{\text{Xe-Xe}} + \delta_{\text{Xe-S}} \quad (2)$$

where δ_0 is the chemical shift of the ^{129}Xe gas at 0 pressure, $\delta_{\text{Xe-Xe}}$ is the interaction term coming from the collision of ^{129}Xe atoms, which can be neglected at low gas pressures, and $\delta_{\text{Xe-S}}$ represents the collision between ^{129}Xe and the pore wall and is therefore dependent on the pore size and the pore surface. As the surface of the pore is constant in the same studied material, the change in δ is inversely proportional to the pore size.

Before performing the ^{129}Xe -NMR experiments, the three prepared cylindrical clay-sand samples with diameters of 7.6 mm

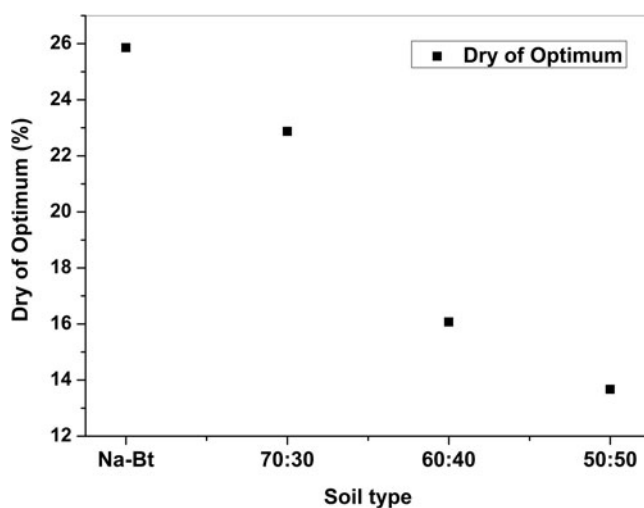


Figure 4. Moisture contents at which the soil substrates were prepared. The 50:50 mix is at a water content that is 10% less than that of pure Na-Bt. Difference between moisture contents of 50:50 mix and pure clay was >10%.

and heights of 20 mm were put into three 8 mm-diameter glass NMR tubes with screw caps. Approximately 1.5 bar of ^{129}Xe gas was introduced into each tube *via* a vacuum system. Xenon enriched at 83% for the 129 isotope was purchased from Eurisotop (France).

The ^{129}Xe spectra were then recorded at room temperature on a narrow-bore 11.7 Tesla spectrometer (Bruker, Germany) equipped with an 8 mm microimaging probe. The experiments were performed by using a one-pulse sequence with a pulse length of 13 μs at a power of 75 W. The spectra were collected with an interscan delay of 50 s. The chemical shift of the free Xe signal was calibrated to $(^{129}\text{Xe} \text{ gas pressure})/2$, which is $1.5/2.0 = 0.75$ ppm (Bonardet *et al.*, 1999). The ^{129}Xe -NMR spectra were fitted by using the program *dmfit* (<https://nmr.cemhti.cnrs-orleans.fr/dmfit/>). The spectra were decomposed into several Lorentzian lines.

Measurement of the adhesive strength of epoxy-coated compacted clay-sand mixtures

Rapid shear tests were performed to evaluate the interfacial shear strength by employing a conventional direct shear apparatus at a displacement rate of 1.25 mm min^{-1} under surcharge loads of 100, 200 and 300 kPa. Failure was allowed to take place along the interface between the epoxy and soil substrate. The interfacial shear strength (τ) was evaluated according to the expression $\frac{P}{A}$, where P is the load cell reading in kN and A is the initial cross-section area in m^2 .

Results and discussion

According to Hölck *et al.* (2012), the critical energy release rate (G_c) when two adhesively bonded surfaces separate is represented by Equation 3:

$$G_c = (w_{12} + w_{\text{chem}})(1 + \phi) + \Delta h \quad (3)$$

The terms w_{12} and w_{chem} represent the physical and chemical bonded interactions between the bonded surfaces. In this study, these are the soil and epoxy surfaces. The contribution of w_{chem} is neglected as there are no suitable sites for chemical bond formation between the two surfaces. Physical interaction is attributed to hydrogen bond interactions between the epoxy functional sites and negatively charged oxygen sites on the clay (Murali *et al.*, 2022). The term $(1 + \phi)$ refers to the surface area available in the form of accessible pores, surface undulations and so on. This aspect of interface formation is the focus of this study. Furthermore, the heat dissipated at the time of debonding of the two surfaces under study is denoted by Δh . The increase in surface area due to the pore-size distribution has a direct correlation with the energy release rate.

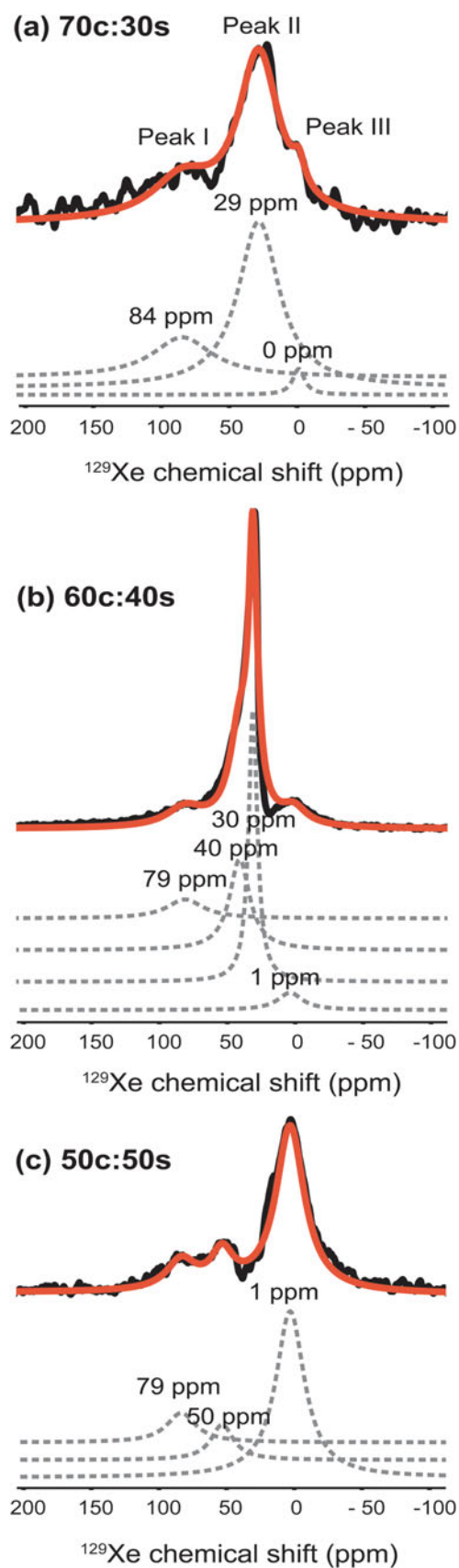


Figure 5. ^{129}Xe -NMR spectra (black solid lines) and the fitted spectra (red solid lines) of (a) 70C:30S, (b) 60C:40S and (c) 50C:50S. The fitted components are plotted as dotted lines.

Table 1. Distribution of porosity in all of the clay-sand mixtures across the entire pore-size regime.

Clay:sand ratio		Peak II			
		Peak I	Component I	Component II	Peak III
70:30	Peak chemical shift (ppm)	84.0	–	29.0	1.0
	Integral percentage (%)	25.0	–	71.8	3.2
60:40	Peak chemical shift (ppm)	79.0	40.0	30.0	1.0
	Integral percentage (%)	13.1	34.5	44.3	8.1
50:50	Peak chemical shift (ppm)	79.0	50.0	–	1.0
	Integral percentage (%)	13.4	12.3	–	74.3

Each of the clay-sand mixtures considered for the further studies was prepared at their ‘dry of optimum’ moisture content. Figure 4 depicts the specific ‘dry of optimum’ for each of the mixtures. There is a difference of 12.19% in moisture content between Na-Bt and the 50:50 mixture. As there are changes in water content in each of these mixtures, the net unbalanced forces on the surfaces of the compacted substrates of each of these mixtures might also vary. According to Goebel *et al.* (2004), the contact angle and surface energy of soils depend on the aggregate fraction and water potential. A key parameter affecting the contact angle and eventually surface energy in soils is the water potential or moisture content. The surface free energies of aggregate and homogenized soils were in the range of 55–65 mJ m^{-1} . Of the polar and dispersive components, the polar component showed variation (32–45 mJ m^{-1}) with aggregate size, whereas the dispersive component remained similar. There are primarily two reasons for the difference in the polar component: first is the availability of clay electron donor locations on the soil surface acting as a base component; and second is the acid component of the surface energy, which is negligible in soils. In the soil mixtures considered, a variation in the base component of the surface energy is expected because both the moisture content and

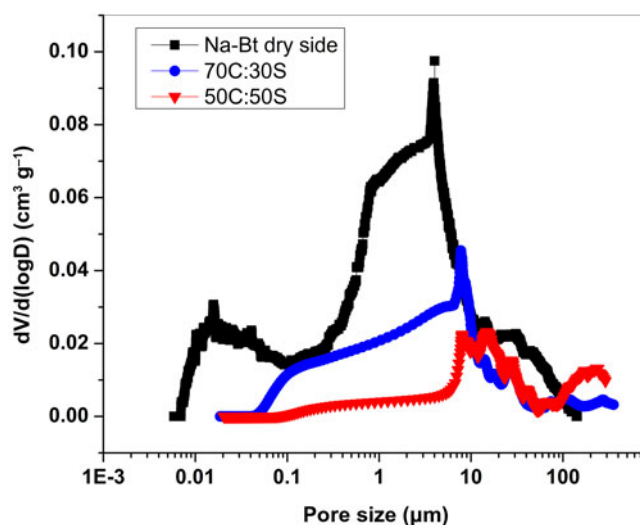


Figure 6. Differential intrusion plot of clay-sand mixtures showing the critical pore entry radius. Pure clay exhibits a higher macropore volume. Clay-sand mixtures gradually shifts to a unimodal distribution as the sand content increases.

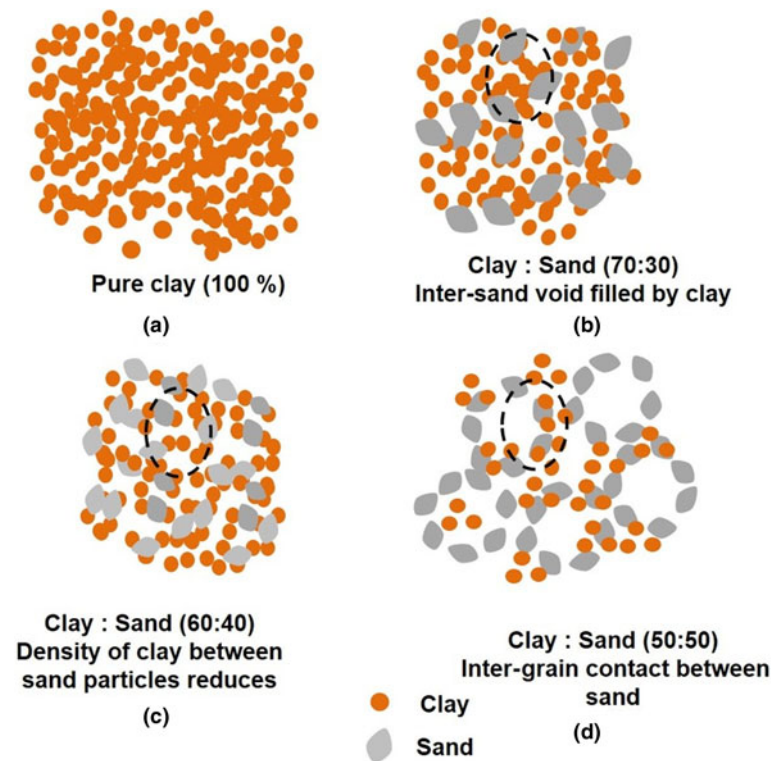


Figure 7. Schematic illustration of porosity variation in clay-sand mixtures: (a) pure clay, (b) 70C:30S with sand particles sparsely populated inside the clay matrix, (c) 60C:40S with the inter-sand space filled by loosely packed clay and (d) 50C:50S with inter-grain contact between sand particles leading to the formation of a partial skeleton of sand. Black dotted circles represent changes in the inter-sand void as the clay content reduces. Adapted from Vallejo & Mawby (2000).

aggregate fraction vary. However, decoupling the individual contributions is not within the scope of this study. More focus is given to changes in surface porosity arising from particle gradation, as explained in the subsequent sections.

^{129}Xe NMR spectra of the clay-sand mixtures

The ^{129}Xe -NMR experimental spectra and the fitted spectra of three samples are shown in Fig. 5. The spectra of all three samples show a signal at 81 ppm. This is attributed to a small space resulting from the ^{129}Xe gas being adsorbed into the clay matrix, which was also found previously in pure clays (Tsiao *et al.*, 1998). In addition, a peak at ~ 1 ppm is also observable for all of the samples. This is attributed to the rapid exchange peak between the free ^{129}Xe gas and the ^{129}Xe gas in the macro-scaled space. The macro-scaled space corresponds mainly to the space between sand particles with size > 50 nm.

The signals in the middle of the spectra are different for the three samples. For the two samples of 50C:50S and 70C:30S, signals appear at 50 and 29 ppm, respectively. A large signal is observed for the sample of 60C:40S, and this is fitted to two Lorentzian lines. The fitted peak chemical shifts of the two compositions were centred close to the middle peaks (Table 1). These two fitted compositions at 40 and 30 ppm were assumed to be a micropore and a macropore, respectively.

For the mixture with the clay-to-sand ratio of 50:50, the peak at 1 ppm dominates, accounting for 74% of the total porosity. This is reasonable as the high sand content leads to a large amount of macro-scaled space amongst the sand particles, so this mixture has a larger average macropore size than the other two mixtures. When more small clay particles were added to increase the clay:sand ratio to 60:40 and 70:30, the middle peak became the main peak, with a proportion of over 71% of the total porosity. This is because more small clay

particles filled the space between large sand particles and the volume of macropores became more filled compared to the 50:50 mixture.

There was an upward shift in the spectra as the clay:sand ratio decreased from 70:30 to 50:50. This was a clear indication of the presence of smaller pores. At a higher clay content, sand particles float within the matrix without any particle-to-particle contact; therefore, the major feature of such a mixture is the presence of mesopores and nanopores from clay aggregates and clay galleries.

Pore-size distribution according to MIP

The information obtained from the ^{129}Xe -NMR spectra provided a qualitative impression of the pore-size distribution in clay-sand mixed soils. Specific details such as critical pore diameter cannot be obtained using this technique. Information on the exact pore entry diameter is essential when analysing interfacial adhesive strength performance. To help us better understand the different pore-size regimes, we used the MIP technique. The pore-size distributions of all soil mixtures were estimated using MIP, and the differential intrusion plot obtained for all of the soil mixtures is shown as in Fig. 6. Mixture 60C:40S is excluded from the intrusion curve based on the findings from interface shear testing, which are given in the next section.

Pure Na-Bt exhibits a bimodal distribution, with a peak at the macropore and mesopore regime. The other soil mixtures gradually shift from a bimodal to a unimodal distribution as the proportion of the mixture varied from 70C:30S to 50C:50S. With equal fractions of clay and sand, we see a predominance of pores of 10–12 μm in the macropore regime and near-zero mercury intrusion in the mesopore regime. The critical pore entry radius obtained for the 50:50 mixture is 17 μm with an intrusion volume of 0.02 $\text{cm}^3 \text{g}^{-1}$. As clay content reduces from 100% to 50%, the critical pore entry radius increases from 4 to 17 μm .

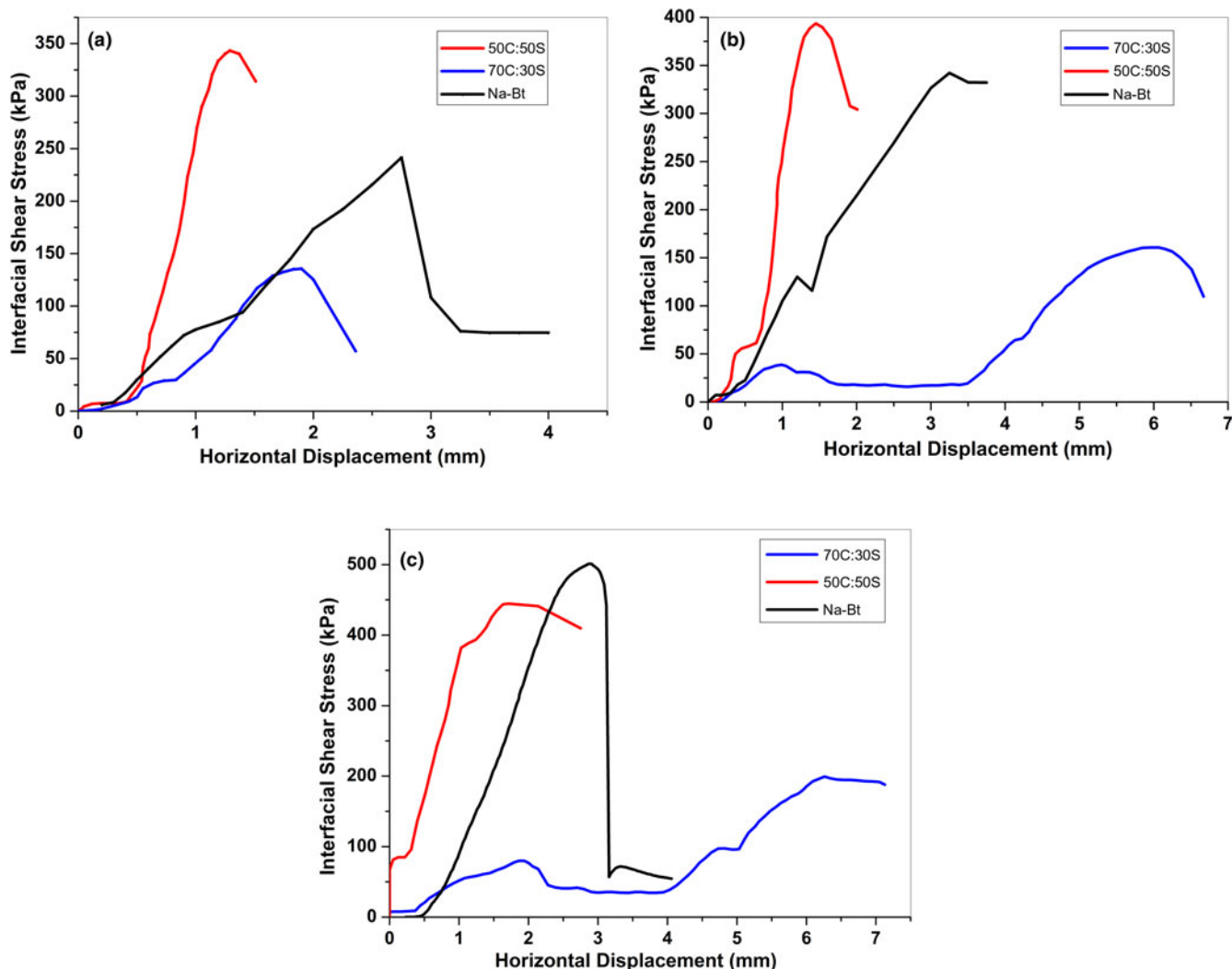


Figure 8. Interfacial adhesive stress vs horizontal displacement obtained for the three epoxy-coated soil mixtures under consideration (Na-Bt, 50C:50S and 70C:30S): (a) 100 kPa, (b) 200 kPa and (c) 300 kPa.

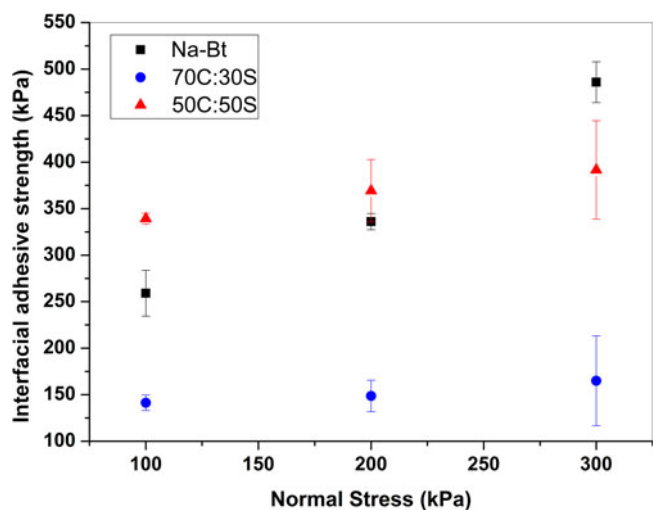


Figure 9. Variation of interfacial adhesive strength with normal stress for all of the soils considered. The 50C:50S mixture shows the highest interfacial adhesive strength at 100 and 200 kPa but not at 300 kPa.

The arrangement of sand within a matrix of clay relates to the percentage of clay content, as depicted in Fig. 7a–d. As a small fraction of clay gets replaced by sand, sand particles become sparsely populated within clay matrix. Afterwards, when the clay fraction reduces, the intergranular space between sand particles becomes smaller and less populated by clay (Fig. 7b). When the clay fraction reduces further, the sand particles attain inter-grain contact. At this stage, very few of the intergranular sand voids are filled with very loosely packed clay, as illustrated in Fig. 7d. For the formation of a partial skeleton of sand, optimal replacement of the clay fraction is required. This study does not focus on achieving the optimal fines content. However, the changes in porosity arising from the arrangement of different grains is considered to be the mechanism underlying the changes in interfacial strength in the various mixtures. This is reflected in the critical pore entry radius of the 50:50 mixture compared to pure Na-Bt. The 50:50 mixture was characterized by a critical pore entry radius of 17 μm compared to 8.14 and 4.00 μm for the 60C:40S and 70C:30S mixtures. This behaviour occurs as small clay grains arrange in a more closely packed manner, reducing the macropore size. However, it is interesting to note the very

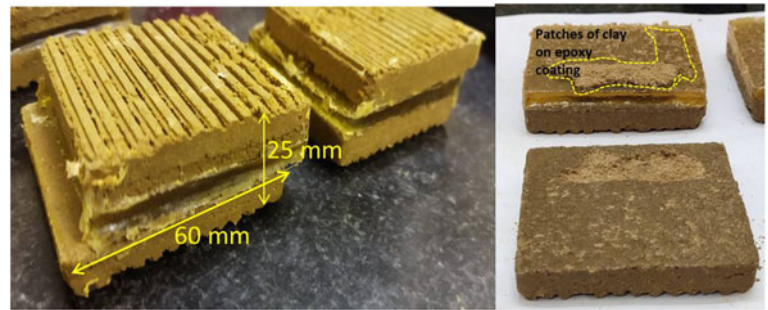


Figure 10. Specimens that failed under shear, clearly showing adhesive failure at the interface.

high intrusion volume (0.09 cc g^{-1}) by mercury in pure Na-Bt. In addition, we did not achieve the threshold fines content value to obtain the greatest interparticle contact between sand particles, as this might not have a positive impact on interfacial bond strength.

The lower particle size of clay grains gives rise to smaller pores when the clay proportion increases from 50% to 100%. In addition, these clay grains exhibit greater porosity compared to the larger, angular sand grains, as demonstrated by their greater intrusion volume. This particular behaviour of clay is attributed to its mineralogy and particle size (Horpibulsuk *et al.*, 2010). For Na-Bt, there are two distinct peaks clearly demarcating the pore-size regimes as macropores ($>50 \text{ nm}$) and mesopores (2–50 nm). Miller & Sower (1958) studied the interfacial strength characteristics of soil–aggregate mixtures. The highest density was obtained at 26% fines and 74% aggregate contents. As the fines content increases beyond a threshold value, the interparticle contact between sand grains reduces, and this can give rise to greater cohesion and lower frictional values (Havens & Goodwin, 1951). The obtained values of the porosity distribution in the clay–sand mixtures agree with the mechanism presented by Miller & Sowers (1958).

Interfacial adhesive strength between the epoxy coating and soil

The interfacial adhesion values between all of the soil mixtures and the epoxy coating were determined to understand the effect of porosity on the adhesion mechanism. Out of all of the

mixtures, that with a clay:sand ratio of 50:50 exhibited the highest interfacial strength for all of the normal stresses, followed by Na-Bt and 70C:30S, respectively, as depicted in Fig. 8. The error bars of interfacial adhesive strength at each normal stress are given in Fig. 9. The underlying reason for this highest strength being exhibited by the 50:50 mixture could be due to the pore-size distribution of the mixture. The macropore regime is broader for the 50:50 mixture, with a macroporosity of 74.3% in comparison to 8.12% in the 60C:40S mixture and 3.21% in the 70C:30S mixture. The highest interfacial strength of 450 kPa was observed at 300 kPa normal stress and is directly correlated with the formation of greater interface thickness (polymer penetration). However, Na-Bt exhibited a slightly higher interfacial adhesive strength at 300 kPa. This increase at higher normal stress is possibly due to increased shear contact area and the extended epoxy deformation occurring inside the pores. Actual epoxy-coated specimens exhibited adhesive failure across the interface, as shown in Fig. 10. Here, the 50:50 mixture exhibited a higher critical pore entry radius than pure Na-Bt, and so greater intrusion by epoxy is possible and therefore so is a greater interface thickness.

The distinct pore microstructure exhibited by the clay–sand mixtures can be linked to the mechanism by which the individual particles are arranged in the soil. As the clay is replaced by sand starting from 30% by weight, we can see a clear shift in pore sizes in the NMR measurements. At sand fractions of 30% and 40%, mesopores predominate. This could be due to the gradual formation of a sand skeleton from a partial to a complete state during the static compaction being applied to the samples. The

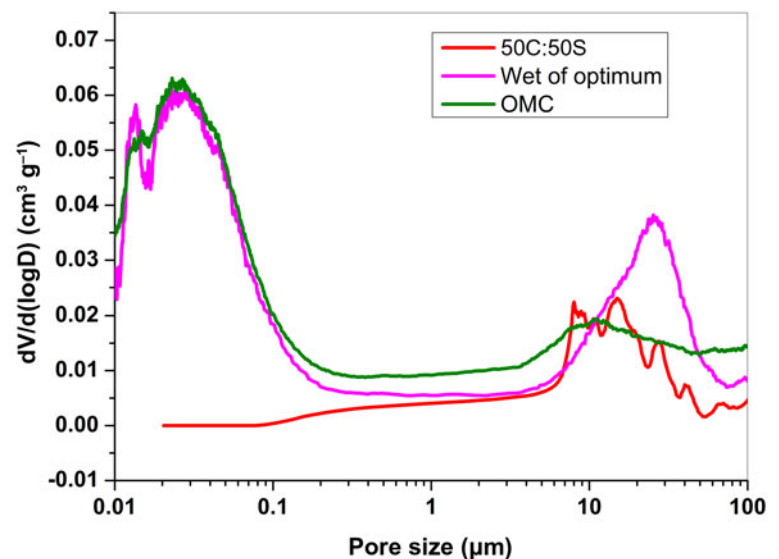


Figure 11. Mercury differential intrusion curves of pure Na-Bt at OMC, 'wet of optimum' moisture content and a clay–sand mixture at 50:50 proportion.

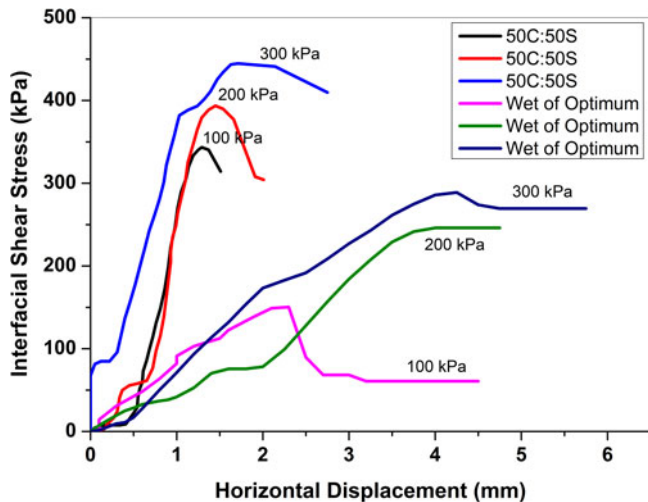


Figure 12. Interfacial adhesive strength exhibited by pure Na-Bt at the ‘wet of optimum’ moisture content and a 50C:50S clay-sand mixture under all of the normal stresses. The clay-sand mixture exhibited higher strength than the pure clay in all of the cases.

compressible behaviour of clay-sand mixtures depends greatly on the transition fines content and intergranular void ratio (Cabalar & Hasan, 2013).

Thus, clay-sand mixtures with higher macroporosities exhibited the highest interfacial adhesive strength. This is primarily attributed to the formation of a thicker diffused interface, as discussed in our earlier work (Murali *et al.*, 2022).

From the differential intrusion curve, the porosity (in the macropore regime) of pure Na-Bt at ‘wet of optimum’ was found to be similar to the clay-sand mixture in a 50:50 composition, as shown in Fig. 11. However, the interfacial bond strength was significantly different between them. Pure Na-Bt at 46.38% water content exhibited a lower interfacial adhesive bond performance at all of the normal stresses compared to the 50:50 mixture, as shown in Fig. 12. Although pure clay is characterized by a bimodal distribution, the critical pore radius at the macropore region was comparable to the clay-sand mixture. Both of these exhibited a critical pore entry radius in the macropore regime: 25.38 μm at 0.038 $\text{cm}^3 \text{g}^{-1}$ intrusion volume for Na-Bt and 17 μm at 0.022 $\text{cm}^3 \text{g}^{-1}$ intrusion volume for the 50:50 mixture. Even with a higher critical pore entry radius at the ‘wet of optimum’ moisture content, the reduction in interfacial performance points to the detrimental effect of moisture content regarding interfacial adhesion. As expressed in the critical energy release rate equation (Equation 3), apart from porosity, physical and chemical interactions also contribute to bond strength. The presence of water might block access to potential interactive sites for non-bonded interactions (hydrogen bonds/van der Waal’s) and bonded interactions, if any, on the soil substrate. Therefore, moisture serves as one of the determining factor for soil porosity and interfacial bond strength development with a polymer coating. The effect of porosity due to changes in particle gradation, however, is reflected in the macroscale interface strength performance.

The macro-mechanical tests conducted on epoxy-coated pure clay and various clay-sand mixtures demonstrated the role of porosity in interface formation. The presence of moisture can be deleterious for interface formation even when larger pores are available for epoxy penetration. Saturated-dry-surface substrates behaved better than wet-surface substrates for interface bonding

with a repair material. The importance of surface roughness, moisture state of the substrate and viscosity of the repair material is highlighted by Bentz *et al.* (2018). In addition, the negative impacts of moisture on interfacial interactions between carbon fibres and an epoxy matrix were investigated *via* molecular dynamics simulation by Tam *et al.* (2023). The masking of epoxy functional sites and fibre surfaces by water layers inhibited the molecular-scale interactions that are essential for building up an interface.

A study of pore distribution in a marine soft soil with varying clay content shows changes in micropores (0.02–0.18 μm) and mesopores (≤ 0.18 –0.78 μm) and very little effect on macroporosity (0.78 μm). An increase in clay content reduced the critical pore entry radius and also led to the absence of macropores and prominence of nanopores in the soil (Jiao *et al.*, 2021). For the clay-sand mixtures, we observed an increase in critical pore entry radius with decreasing clay content. The overall porosity in clays treated with boric acid was previously found to be ~65%, with an average macropore diameter in the range of 2–10 μm (Kokunešoski *et al.*, 2016). These works are in line with the macropore distribution obtained in this work for pure clay at a higher water content.

Conclusions

The interfacial adhesive strengths between different clay-sand mixtures and an epoxy coating were evaluated in this study. The greatest strength was demonstrated by a clay-sand mixture of 50:50 composition, thus reflecting the role of porosity in interfacial strength. Pure clay and a clay-sand mixture of 50:50 composition exhibited similar porosity but different interfacial adhesion strengths. This points to the negative impact of moisture on interfacial strength. A deeper understanding of porosity distribution in various clay-sand compositions through MIP and ^{129}Xe -NMR was provided in this work. A clay-sand mixture of 50C:50S composition had a macroporosity of 74.3%, and the mixture of 70C:30S composition had only 3.21% macroporosity. MIP revealed the exact critical pore entry radii for all of the mixtures. The nanopores inside the clay matrix were evidenced in the ^{129}Xe -NMR spectra. Although these pore regimes are not beneficial for interfacial strength development (larger epoxy molecules cannot penetrate into these minute pores), their identification could be helpful in applications involving gaseous particle transport and storage (Hu *et al.*, 2018; Luo *et al.*, 2022) for methane adsorption or carbon dioxide storage, for example.

Author contributions. Nidhi Murali: Conceptualization, Methodology, Formal Analysis, Writing – Original Draft. Jing Li: Methodology (^{129}Xe -NMR), Formal Analysis, Writing – Original Draft. Anvi Agarwal: Methodology. Patrick Berthault: Supervision, Methodology. Pijush Ghosh: Supervision, Funding Acquisition.

Financial support. The authors would like to acknowledge the financial support from the Science and Engineering Research Board, Government of India, for supporting this work (Project No. CRG/2019/003554).

Conflicts of interest. The authors declare none.

References

- Agus S.S., Schanz T. & Fredlund D.G. (2010) Measurements of suction versus water content for bentonite-sand mixtures. *Canadian Geotechnical Journal*, 47, 583–594.

- Bentz D.P., De la Varga I., Muñoz J.F., Spragg R.P., Graybeal B.A., Hussey D.S. et al. (2018) Influence of substrate moisture state and roughness on interface microstructure and bond strength: slant shear vs. pull-off testing. *Cement and Concrete Composites*, **87**, 63–72.
- Bonardet J.L., Fraissard J., Gédéon A. & Springuel-Huet M.A. (1999) Nuclear magnetic resonance of physisorbed ^{129}Xe used as a probe to investigate porous solids. *Catalysis Reviews – Science and Engineering*, **41**, 115–225.
- Briceno C., Azenha M., Vasconcelos G. & Lourenço P.B. (2024) Influence of conditioning of clay bricks over shear strength of brick masonry. *Journal of Building Engineering*, **82**, 108138.
- Cabalar A.F. & Hasan R.A. (2013) Compressional behaviour of various size/shape sand–clay mixtures with different pore fluids. *Engineering Geology*, **164**, 36–49.
- Carrero-González B., Carrero-González B., de la Cruz M.T. & Casermeiro, M.Á. (2012) Application of magnetic resonance techniques to evaluate soil compaction after grazing. *Journal of Soil Science and Plant Nutrition*, **12**, 165–182.
- Chen K. & Liang F. (2024) Experimental investigation on the dynamic shear behavior of the unsaturated soil–concrete interface under cyclic loading. *Soil Dynamics and Earthquake Engineering*, **176**, 108325.
- Cuthbertson A.J.S., Samsami F. & Dong P. (2018) Model studies for flocculation of sand–clay mixtures. *Coastal Engineering*, **132**, 13–32.
- Di Donna A., Ferrari A. & Laloui L. (2016) Experimental investigations of the soil–concrete interface: physical mechanisms, cyclic mobilisation and behaviour at different temperatures. *Canadian Geotechnical Journal*, **53**, 659–672.
- Duan P., Shui Z., Chen W. & Shen C. (2013) Effects of metakaolin, silica fume and slag on pore structure, interfacial transition zone and compressive strength of concrete. *Construction and Building Materials*, **44**, 1–6.
- Feng D., Li X., Wang X., Li J., Sun F., Sun Z. et al. (2018) Water adsorption and its impact on the pore structure characteristics of shale clay. *Applied Clay Science*, **155**, 126–138.
- Filimonova S., Nossov A., Dümig A., Gédéon A., Kögel-Knabner I. & Knicker H. (2011) Evaluating pore structures of soil components with a combination of ‘conventional’ and hyperpolarised ^{129}Xe NMR studies. *Geoderma*, **162**, 96–106.
- Goebel M.-O., Bachmann J., Woche S.K., Fischer W.R. & Horton R. (2004) Water potential and aggregate size effects on contact angle and surface energy. *Soil Science Society of America Journal*, **68**, 383–393.
- Gujar P., Alex A., Santhanam M. & Ghosh P. (2021) Evaluation of interfacial strength between hydrating cement paste and epoxy coating. *Construction and Building Materials*, **279**, 122511.
- Gujar P., Murali N., Ilango N.K., Santhanam M. & Ghosh P. (2023) Engineering interfacial strength of polymer coated hydrating cement paste by tuning calcium characteristics. *Materials and Structures/Materiaux et Constructions*, **56**, 65.
- Havens J.H. & Goodwin W.A. (1951) *Clay Mineralogy and Soil Stabilization*. Kentucky Transportation Center Research Report, 1346. Retrieved from https://uknowledge.uky.edu/krc_researchreports/1346
- Hölck O., Bauer J., Wittler O., Michel B. & Wunderle B. (2012) Comparative characterization of chip to epoxy interfaces by molecular modeling and contact angle determination. *Microelectronics Reliability*, **52**, 1285–1290.
- Horpibulsuk S., Rachan R., Chinkulkijniwat A., Raksachon Y. & Suddepong A. (2010) Analysis of strength development in cement-stabilized silty clay from microstructural considerations. *Construction and Building Materials*, **24**, 2011–2021.
- Hou Y., Wang B., Huang L., Xu J., Liu D. & Jiahua Z. (2021) Microstructure and macromechanical properties of retaining structure of near-water reinforced soil under dry–wet cycle. *Mathematical Problems in Engineering*, **2021**, 6691278.
- Hu H., Xing Y. & Li X. (2018) Molecular modeling on transportation of CO_2 in montmorillonite: diffusion and permeation. *Applied Clay Science*, **156**, 20–27.
- Ilango N.K., Gujar P., Nagesh A.K., Alex A. & Ghosh P. (2021) Interfacial adhesion mechanism between organic polymer coating and hydrating cement paste. *Cement and Concrete Composites*, **115**, 103856.
- Jiao W., Zhou D. & Wang Y. (2021) Effects of clay content on pore structure characteristics of marine soft soil. *Water (Switzerland)*, **13**, 1–19.
- Khajeh A., Jamshidi Chenari R., Payan M. & MolaAbasi H. (2023) Assessing the effect of lime-zeolite on geotechnical properties and microstructure of reconstituted clay used as a subgrade soil. *Physics and Chemistry of the Earth, Parts A/B/C*, **132**, 103501.
- Kokunešoski M., Šaponjić A., Stanković M., Majstorović J., Egelja A., Ilić S. & Matović B. (2016) Effect of boric acid on the porosity of clay and diatomite monoliths. *Ceramics International*, **42**, 6383–6390.
- Li J., Mailhiot S., Sreenivasan H., Kantola A.M., Telkki V.-V. & Kinnunen P. (2022) ^{129}Xe NMR analysis reveals efficient gas transport between inborn micro-, meso- and macropores in geopolymers. *Cement and Concrete Research*, **155**, 106779.
- Lubelli B., de Winter D.A.M., Post J.A., van Hees R.P.J. & Drury M.R. (2013) Cryo-FIB-SEM and MIP study of porosity and pore size distribution of bentonite and kaolin at different moisture contents. *Applied Clay Science*, **80–81**, 358–365.
- Luo Q., Li Y., Zhang Z., Peng X. & Geng G. (2022) Influence of substrate moisture on the interfacial bonding between calcium silicate hydrate and epoxy. *Construction and Building Materials*, **320**, 126252.
- Miller E.A. & Sowers G. (1958) The strength characteristics of soil–aggregate mixtures & discussion. *Highway Research Board Bulletin*, **183**, 16–32.
- Murali N., Gujar P. & Ghosh P. (2022) Performance of clay–epoxy interface at different points on proctor curve. *Applied Clay Science*, **226**, 106553.
- Orts W.J., Roa-Espinosa A., Sojka R.E., Glenn G.M., Imam S.H., Erlacher K. & Pedersen J.S. (2007) Use of synthetic polymers and biopolymers for soil stabilization in agricultural, construction, and military applications. *Journal of Materials in Civil Engineering*, **19**, 58–66.
- Pan J., Wang B., Wang Q., Ling X., Fang R., Liu J. & Wang Z. (2023) Thickness of the shear band of silty clay–concrete interface based on the particle image velocimetry technique. *Construction and Building Materials*, **388**, 131712.
- Shafizadeh A., Gimmi T., Van Loon L.R., Kaestner A.P., Mäder U.K. & Churakov S.V. (2020) Time-resolved porosity changes at cement–clay interfaces derived from neutron imaging. *Cement and Concrete Research*, **127**, 105924.
- Soltani-Jigheh H., Bagheri M. & Amani-Ghadim A.R. (2019) Use of hydrophilic polymeric stabilizer to improve strength and durability of fine-grained soils. *Cold Regions Science and Technology*, **157**, 187–195.
- Tam L., Ntjam Minkeng M.A., Lau D., Mansour W. & Wu C. (2023) Molecular interfacial shearing creep behavior of carbon fiber/epoxy matrix interface under moisture condition. *Engineering Fracture Mechanics*, **282**, 109177.
- Tripathi K.K. & Viswanadham B.V.S. (2012) Evaluation of the permeability behaviour of sand–bentonite mixtures through laboratory tests. *Indian Geotechnical Journal*, **42**, 267–277.
- Tsiao C.-J., Carrado K.A. & Botto R.E. (1998) Investigation of the microporous structure of clays and pillared clays by ^{129}Xe NMR. *Microporous and Mesoporous Materials*, **21**, 45–51.
- Vallejo L. E. & Mawby R. (2000) Porosity influence on the shear strength of granular material–clay mixtures. *Engineering Geology*, **58**, 125–136.
- Wang Y.B., Zhao C. & Wu Y. (2020) Study on the effects of grouting and roughness on the shear behavior of cohesive soil–concrete interfaces. *Materials*, **13**, 3034.
- Watabe Y., Yamada K. & Saitoh K. (2011) Hydraulic conductivity and compressibility of mixtures of Nagoya clay with sand or bentonite. *Geotechnique*, **61**, 211–219.
- Wu Y., Zhang X., Zhao C. & Zhao C. (2023) Effects of soil unloading and grouting on the vertical bearing mechanism for compressive piles. *Ocean Engineering*, **271**, 113754.
- Xia W., Wang Q., Yu Q., Yao M., Sun D., Liu J. & Wang Z. (2023) Experimental investigation of the mechanical properties of hydrophobic polymer-modified soil subjected to freeze–thaw cycles. *Acta Geotechnica*, **18**, 3623–3642.
- Zhu H., Li S., Hu Z., Ju Y., Pan Y., Yang M. et al. (2023) Microstructural observations of clay-hosted pores in black shales: implications for porosity preservation and petrophysical variability. *Clay Minerals*, **58**, 310–323.